Vision Research 51 (2011) 447–458

Contents lists available at ScienceDirect

Vision Research

journal homepage: www.elsevier.com/locate/visres

A mouse M-opsin monochromat: Retinal cone photoreceptors have increased M-opsin expression when S-opsin is knocked out

Lauren L. Daniele [a], Christine Insinna [a], Rebecca Chance [b], Jinhua Wang [c], Sergei S. Nikonov [d], Edward N. Pugh Jr. [a,*]

[a] Center for Neuroscience, University of California, Davis, United States
[b] Graduate Program in Neuroscience, University of Pennsylvania, United States
[c] Department of Dermatology, University of Pennsylvania, United States
[d] Department of Neuroscience, University of Pennsylvania, United States

ARTICLE INFO

Article history:
Received 12 October 2010
Received in revised form 23 December 2010
Available online 8 January 2011

Keywords:
Opsin
Cone survival
Phototransduction
Color vision

ABSTRACT

Mouse cone photoreceptors, like those of most mammals including humans, express cone opsins derived from two ancient families: S-opsin (gene *Opn1sw*) and M-opsin (gene *Opn1mw*). Most C57Bl/6 mouse cones co-express both opsins, but in dorso-ventral counter-gradients, with M-opsin dominant in the dorsal retina and S-opsin in the ventral retina, and S-opsin 4-fold greater overall. We created a mouse lacking S-opsin expression by the insertion of a Neomycin selection cassette between the third and fourth exons of the *Opn1sw* gene ($Opn1sw^{Neo/Neo}$). In strong contrast to published results characterizing mice lacking rhodopsin ($Rho^{-/-}$) in which retinal rods undergo cell death by 2.5 months, cones of the $Opn1sw^{Neo/Neo}$ mouse remain viable for at least 1.5 yrs, even though many ventral cones do not form outer segments, as revealed by high resolution immunohistochemistry and electron microscopy. Suction pipette recordings revealed that functional ventral cones of the $Opn1sw^{Neo/Neo}$ mouse not only phototransduce light with normal kinetics, but are more sensitive to mid-wavelength light than their WT counterparts. Quantitative Western blot analysis revealed the basis of the heightened sensitivity to be increased M-opsin expression. Because S- and M-opsin transcripts must compete for the same translational machinery in cones where they are co-expressed, elimination of S-opsin mRNA in ventral $Opn1sw^{Neo/Neo}$ cones likely increases M-opsin expression by relieving competition for translational machinery, revealing an important consequence of eliminating a dominant transcript. Overall, our results reveal a striking capacity for cone photoreceptors to function with much reduced opsin expression, and to remain viable in the absence of an outer segment.

1. Introduction

1.1. Photoreceptor viability and outer segment structure may depend on opsin expression

Vertebrate retinal photoreceptors initiate vision via a G-protein coupled receptor (GPCR) cascade whose molecular components are concentrated within their outer segments, whose renewal gives rise to a distinctive daily burden of transcription, translation, protein trafficking and turnover. The outer segments comprise a dense stack of lamellar membranes packed with opsin GPCR at a membrane density of ~25,000 μm^{-2}, among the highest of all membrane proteins, and are renewed at a rate of about 10% per day, (Hollyfield, 1979; Young, 1967, 1971). Rod photoreceptors require substantial opsin expression for the elaboration of functioning outer segments, and ultimately for cell viability: rods of mice from which rhodopsin has been genetically deleted ($Rho^{-/-}$) form only rudimentary cilia-like outer segments with no disc structure, and eventually undergo apoptosis, leading to severe retinal degeneration by age 2.5 months (Humphries et al., 1997; Lee, Burnside, & Flannery, 2006). Cone photoreceptors also fail to elaborate outer segments when their opsins fail to traffic normally, and subsequently undergo rapid degeneration (Zhang et al., 2008; Znoiko et al., 2005). These observations have led to the hypothesis that photoreceptor viability requires normal opsin expression and outer segment structure, but this has not been tested in cones.

1.2. Analysis of cone opsin knockouts is complicated by the coexpression of cone opsins in dorsal – ventral countergradients

In principle, this hypothesis could be tested in mice by knocking out one of the two distinct cone opsins, short-wave sensitive opsin (S-opsin; gene *Opn1sw*) or mid-wave opsin (M-opsin; *Opn1mw*).

* Corresponding author. Address: Department of Physiology, Center for Neuroscience, University of California, Davis, 1544 Newton Court, Davis, CA 95618, United States.
E-mail address: enpugh@ucdavis.edu (E.N. Pugh).

0042-6989/$ - see front matter © 2011 Elsevier Ltd. All rights reserved.
doi:10.1016/j.visres.2010.12.017

However, the matter is complicated by the facts that most mouse cones co-express both opsins, and that the relative expression of the two opsins follows a dual dorso-ventral gradient, with M-opsin dominant in the most dorsal retina, and S-opsin dominant elsewhere (Applebury et al., 2000; Nikonov, Kholodenko, Lem, & Pugh, 2006; Szel, Lukats, Fekete, Szepessy, & Rohlich, 2000). Thus, understanding the consequences of deleting one of the cone opsins requires detailed consideration of the gradients of expression.

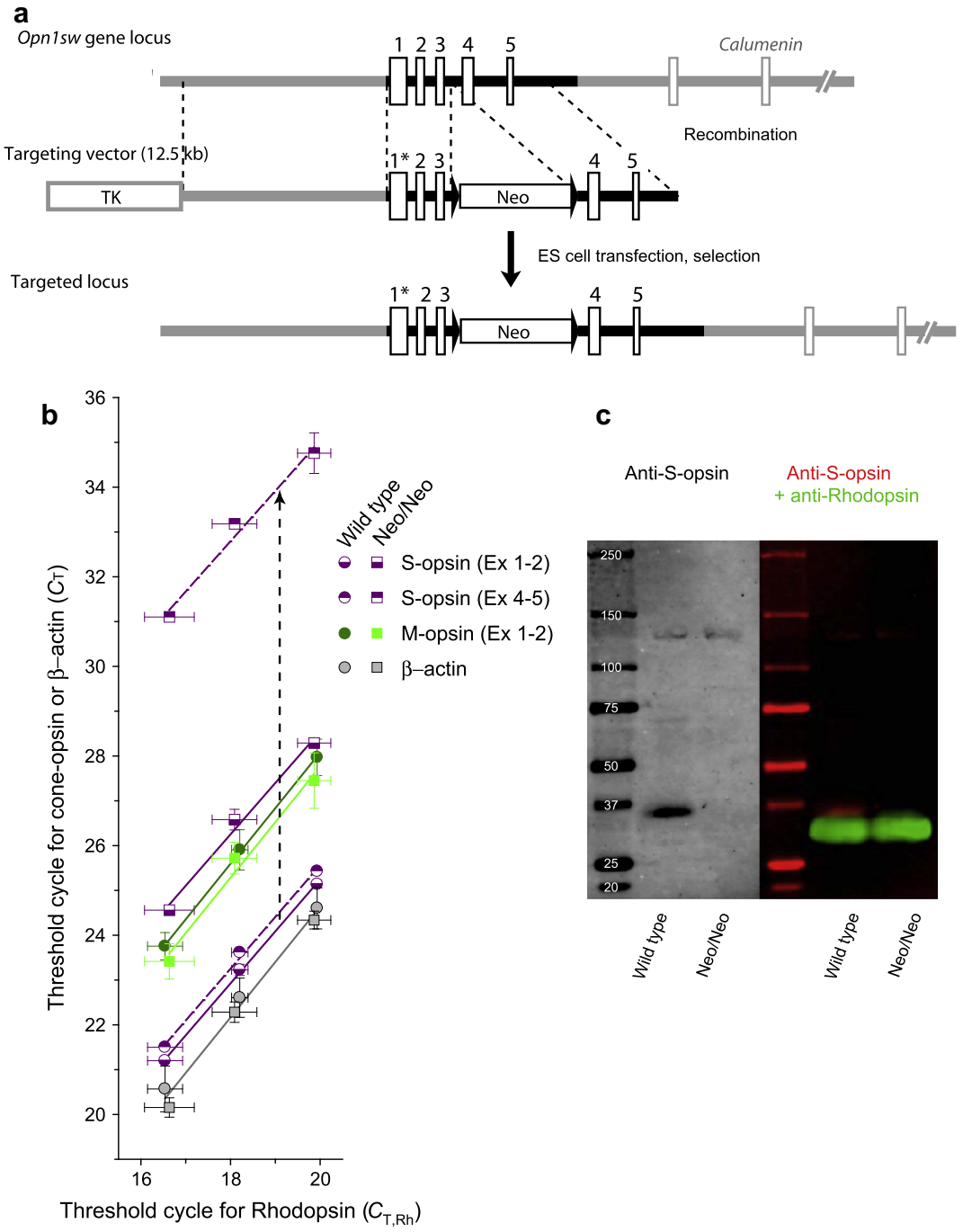

Fig. 1. S-opsin knock-in targeting strategy created a severely hypomorphic allele (*Opn1sw*^{Neo}): (a) *Schematic of Opn1sw targeting strategy*. The targeting vector comprised a Neomycin resistance cassette (Neo) flanked by FRT recombination sites (arrowheads) and homologous sequences (4.5 Kb 3′ and 816 bp 5′) to the *Opn1sw* gene locus (the calumenin gene, which abuts the 5′ end of the *Opn1sw* gene and is transcribed in the reverse direction on the complementary strand). The asterisk indicates the site of a targeted point mutation. Southern blotting and PCR confirmed successful targeting. (b) *Real-time quantitative PCR results*. The threshold cycle (C_T) of Taq-Man PCR reactions with primers for S-opsin (purple), M-opsin (green) and β-actin (gray) message are plotted against C_T for reactions with primers for rhodopsin message. Three dilutions of cDNA templates generated from *Opn1sw*$^{Neo/Neo}$ (squares) and WT littermate control (circles) served as the input to the PCR reactions. Primer sequences spanned exon junctions 1–2 (filled or bottom half-filled) or 4–5 (top half-filled) symbols. Data were obtained from mRNA extracted from the entire eyes of an *Opn1sw*$^{Neo/Neo}$ and a WT littermate control. Error bars are standard deviations: observations with 1× dilution of the cDNA from the reverse transcriptase reaction were replicated 2× for each data point, those with ¼ dilution 4× and those with 1/16 dilution 8×. The straight lines, fitted by least-squares to the data, are very nearly parallel (slopes varied by 10%, ranging from 1.13 to 1.24), so that the vertical offset of the lines representing the same transcript in *Opn1sw*$^{Neo/Neo}$ and WT retinas provide load-independent estimates of differences in the transcripts. (c) *Immunoblotting with an anti-S-opsin antibody detects no S-opsin in the Opn1sw*$^{Neo/Neo}$ *retina*. Extracts of WT and *Opn1sw*$^{Neo/Neo}$ retinas containing 60 pmol rhodopsin (corresponding to ~10% of the total retina) were loaded into adjacent gel lanes, and probed with antibodies for S-opsin (left panel, grayscale presentation), or for S-opsin (right panel, red) and rhodopsin (green). No S-opsin is detected in the *Opn1sw*$^{Neo/Neo}$ retina lane. Control experiments (Supplement, Fig. 1S) show that ~30 fmol S-opsin would be detectable.

We have generated a mouse that expresses no detectable S-opsin (*Opn1sw*$^{Neo/Neo}$). This S-opsin deficient mouse provides a novel model in which the dependence of the survival of photoreceptors on the expression of opsin can be examined. Because of the dorso-ventral gradient of co-expression of M-opsin in wild-type (C57Bl/6) mouse cones, the *Opn1sw*$^{Neo/Neo}$ mouse also provides a model for examining the specific opsin requirement for the formation of functional outer segments. Our results show that the cones of the *Opn1sw*$^{Neo/Neo}$ mouse express only M-opsin, and that many of its ventral cones have elevated M-opsin expression relative to wild-type and can generate light responses with normal kinetics. Remarkably, many other more ventral cones fail to elaborate outer segments altogether, yet remain viable, such that the S-opsin deficient mouse maintains a full complement of cones into adulthood.

2. Materials and methods

2.1. Generation of *Opn1sw*$^{Neo/Neo}$ mice

The mouse short wavelength sensitive opsin gene (*Opn1sw*) was cloned from a mouse genomic library with an *Escherichia coli* based method for recombination cloning and *in vivo* library screening (Zhang, Li, & Elledge, 2002). A *flox*ed tetracycline resistance (Tc^R) fragment flanked by homology to *Opn1sw* intron 3 was generated by PCR (Expand High Fidelity PCR Kit, Roche Labs, 1732641) and ligated into pLM179 at the pme-I site. The following primers (5′–3′) were used for PCR to create the Tc^R homology insert used to screen a λ-phage library (λ-KO-2) for *Opn1sw in vivo* (Zhang et al., 2002).

Opn1sw-TC1: GGGTTTTGAGAGGGGCAGGTAGGAGTAACTCAGG AGGCCCCAGGAGAGACAAGCGCGCAATTAACCCTCACTAAAG.
Opn1sw-TC2: TCCTATCTGACCACGGATATTCTAGACGTATCCTGA GGAAGATATATACGAGAGCGCGCGTAATACGACTCAC.

Sequencing confirmed a Tc-resistant clone containing ~8 Kb of a genomic DNA sequence including *Opn1sw*. The Tc^R insert was removed from the clone with Cre recombinase and a point mutation generating an F81Y residue change was introduced with a Stratagene QuickChange site-directed mutagenesis kit (cat # 200518, Agilent Technologies, Santa Clara, CA 95051). (A detailed description of the consequences of the F81Y mutation will be presented in another report.)

A DNA fragment was created by PCR from pKOEZ71 with the following primers.

Opn1sw-NEO1: GGGTTTTGAGAGGGGCAGGTAGGAGTAACTCAG GAGGCCCCAGGAGAGACAGCTGATCAACAGATCCTCTACGC.
Opn1sw-NEO2: TCCTATCTGACCACGGATATTCTAGACGTATCCTG AGGAAGATATATACGCAAGGGCTGCTAAAGGAAG.

This fragment contained the FRT flanked Neomycin resistance cassette (Neo^R) bounded by short sequences of homology to *Opn1sw* intron 3. To make the final targeting vector (Fig. 1) this DNA fragment was electroporated into RED recombination proficient *E. coli* which already expressed the cloned, mutated *Opn1sw*. The targeting vector 5′ and 3′ homology arms consisted of 5.1 Kb and 1.3 Kb of genome sequence respectively, encompassing most of the *Opn1sw* gene.

ES cells (129S6/SvEvTac) were electroporated with Pvu-I linearized targeting vectors and selected for Neomycin resistance. Genomic DNA was isolated from ~300 G418 resistant clones were screened by PCR and a single recombinant-positive clone, F15 was selected for further analysis. Verification of the F81Y mutation (encoded by a TTC to TAC codon switch) was made by sequencing and presence of correctly targeted *Opn1sw* was confirmed in DNA from F15 by Southern blotting. Probes used for Southern blotting were amplified from mouse genomic and BAC DNA. DNA extracted from ES cell clones was digested with BamH1 and Xho1 and reacted with 5′ and 3′ probes respectively, to distinguish between targeted vs. WT loci.

A single ES cell clone was injected into day 4 C57BL/6J mouse blastocysts followed by implantation into pseudo pregnant female mice by the University of Pennsylvania Transgenic and Chimeric Mouse Core Facility. Highly chimeric mice were bred against C57BL/6J mice and agouti founders were screened by PCR and Southern blotting prior to further breeding. Mice homozygous for the Neo insertion were maintained as breeders and bred against C57BL/6J to create heterozygous mice that were in turn used to create *Opn1sw*$^{Neo/Neo}$ and WT littermate controls for experiments. Unless specifically stated otherwise, all mice used for the experiments reported here were of 1.5–8 months of age.

2.2. Quantitation of Opn1sw transcripts with qRT-PCR

Total RNA was extracted from whole mouse eyes in Eppendorf tubes with plastic homogenizers using the Tri Reagent® (Molecular Research Center, Inc., Cincinnati, Ohio 45212). After DNAase treatment (DNA-free™ kit, Applied Biosystems/Ambion Austin, TX 78744-1832) cDNA was amplified from oligo-dT primed total RNA (0.5 μg) (SuperScript® First-Strand Synthesis System for RT-PCR, Invitrogen Co., # 11904-018, Carlsbad, California 92008). TaqMan® real time qRT-PCR was performed on serial dilutions of cDNA from *Opn1sw*$^{Neo/Neo}$ and WT littermate eyes with a TaqMan 7500 Real-Time PCR System (Applied Biosystems/Life Technologies Corporation, Carlsbad, California 92008) using probes for mouse visual opsins and β-actin (exon boundary and catalogue number): rhodopsin (1-2) Mm00520345-m1; M-opsin (1-2) Mm01193546-m1; S-opsin (1-2) Mm01135619_g1; S-opsin (4-5) Mm00432058_m1; β-actin, Mm 00607939-s1. The experimental strategy produced (for each of two eyes analyzed per genotype) 1 reaction volume of cDNA per primer pair at the undiluted concentration, 2 per pair at 4-fold dilution of cDNA, and 4 per pair at 16-fold cDNA dilution; the primer concentrations were the same in all reactions. The total RNA from each eye used was equated at 5 μg in 15 μl for each reverse transcriptase reaction.

2.3. Quantitation of cone opsins with Western blotting

Mice were dark adapted overnight. Retinas were dissected in darkness with a microscope equipped with an infra-red illuminator and viewers. Protein was extracted from isolated retinas in ~150 μL of a 20 mM Bis–Tris propane buffer (pH 7.5) containing 10 mM dodecyl-β-Maltoside and 5 mM NH_2OH, supplemented with complete Mini protease inhibitor cocktail tablets (1/10 mL, Roche). Protein was extracted by homogenization with 5–10 brief pulses at 3–5 W from a sonifier (Microson XL-2000 ultrasonic cell disrupter, Misonix, Inc. Farmingdale, NY), followed by centrifugation (Eppendorf model 5417 R) at 21,000*g* for 5 min to clear insoluble material from lysates. The rhodopsin concentration of the lysate supernatant was estimated with bleaching difference spectroscopy, as previously described (Lyubarsky, Daniele, & Pugh, 2004). Lysate stocks at 3–4 μM rhodopsin concentration for PAGE were made by adding appropriate amounts of Novex® Tris–Glycine SDS Sample Buffer (2×) (Invitrogen Co., Carlsbad, California 92008, # LC2676). Incremental dilutions of lysate, matched across genotypes for rhodopsin mass, were loaded in Novex® 4–12% Tris–Glycine pre-cast gels (Invitrogen). Gels were transferred onto PVDF membranes and blotted with polyclonal antibodies against mouse cone opsins (described below) and rhodopsin (4D2; Laird & Molday, 1988). Immunopositive bands were probed with LI-COR IRDye® secondary antibodies (#926-32212 800CW Donkey anti-Mouse and # 926-68021 680LT Goat anti-Rabbit, LI-COR Biosciences, Lincoln,

Nebraska 68504-0425). Immunolabeled membranes were visualized with a LI-COR® Odyssey Infra-red imaging system (LI-COR Lincoln, Nebraska 68504-0425). As the masses of cone opsins relative to rhodopsin can be expected to be constant for mice of a given genotype with healthy retinas, spectroscopic quantification of rhodopsin provides a sensitive and accurate means of comparing cone opsin expression levels across genotypes. The total quantity of cone opsin in the adult WT mouse retina can be estimated to be about 10 pmol, about 1/70th that of rhodopsin (Supplement).

Quantification of Western blot signals relative to the rhodopsin mass of lysate loads is commonly used in investigations that assay the quantities of other rod and cone proteins. Among the advantages of this approach are that rhodopsin is the most highly expressed photoreceptor protein, that it is expressed in a tightly regulated concentration in healthy rods (~3 mM relative to the outer segment envelope volume), and that it can be precisely measured with spectroscopy. Thus, rhodopsin serves as an ideal ratiometric marker for photoreceptor layer proteins. However, as Western blot signals are conventionally reported relative to total protein mass input per lane, we also calibrated retinal lysate load mass with the Bradford reagent assay (Bradford, 1976) (Fermentas, Vancouver, BC) using BSA as a standard. A linear calibration series yielded a ratio of 4.2 pmol rhodopsin per μg total retinal protein. This calibration implies that an adult C567Bl/6 retina containing 700 pmol rhodopsin (Lyubarsky et al., 2004) has 170 μg total protein.

2.4. S- and M-opsin antibodies used in immunoblotting

This investigation employs a novel affinity-purified polyclonal antibody raised in rabbits against a C-terminal peptide (amino-acids 317–333, CRKPMADESDVSGSQKT) of mouse S-opsin (Yenzym Antibodies, San Francisco). We also used antibodies raised against N-terminal peptides of S- and M-opsin (Zhu et al., 2003). Dual label immunoblot experiments with a mouse monoclonal antibody raised against rhodopsin established the ability of the novel antibody to discriminate S-opsin from rhodopsin.

2.5. Immunohistochemistry

2.5.1. Precise orientation of enucleated mouse eyes within dorsal–ventral/nasal–temporal coordinates

Mouse eyecups were oriented prior to fixation for retinal cryosectioning, flatmount preparations and electron microscopy using the method of Wagner, McCaffery, and Drager (2000). Briefly, dorsal–ventral and nasal-temporal coordinates are delineated by four large branches of choroidal vessels apparent through the sclera at the rear of the globe. A characteristic asymmetry in the point at which the optic nerve emerges with respect to these coordinates provided a reliable method to orient the eyecups.

2.5.2. Immunohistochemistry analysis of retinal cryosections

Mice were sacrificed, and eyes enucleated with a fine blade followed by immersion fixation in 4% paraformaldehyde or 4% paraformaldehyde 0.5% Glutaraldehyde in 1× phosphate buffered saline at 2–3 h RT or overnight at 4 °C. The anterior segment was cut away with fine scissors and the lens removed. Eyecups were subjected to cryoprotection in PBS containing graded sucrose (10–30% w/v). Cryosections were incubated with Alexa 488-peanut agglutinin (PNA) and a polyclonal antibody to cone arrestin (Zhu et al., 2002) or S-opsin (see above) overnight at 4% with PBS buffer containing BSA (0.5%) and Triton X-100 (0.1%). A secondary antibody (Alexa 555 Goat anti-rabbit) was used to detect immunoreactivity. Immunofluorescent labeling of tissue was visualized with a Zeiss LSM 510 confocal microscope (Zeiss Microscope Imaging, Inc., Thornwood, NY). Images were exported in TIF format with LSM Image Browser software.

2.5.3. Immunohistochemical analysis of retinal flat mounts

Mouse eyes were fixed for retinal flatmounting in the same manner as for cryosections (see above), with the exception that glutaraldehyde was omitted from fixative. Cuts were made to mark the orientation of the retina within the eyecup before the retina was separated from the sclera. Retinal flatmounts were labeled with AlexaFluor 488 conjugate of peanut agglutinin (PNA, Invitrogen/Molecular Probes) and a commercially available polyclonal antibody raised against the bovine cone transducin alpha subunit, $G\alpha_{tc}$ (Santa Cruz Biotechnology, Inc., Santa Cruz, CA. 95060, # s.c. 390 Lot # F0904) using the same buffer and incubation times as above. The isolated retinas were cut with a fine blade to flatten, then mounted with a coverslip on a microscope slide, and imaged with a Nikon Eclipse TE2000-U microscope equipped for epifluorescence. Cone densities were initially determined from images with a feature detection algorithm within ImageJ software (Rasband WS, ImageJ, US National Institutes of Health, Bethesda, MD, USA, http://rsb.info.nih.gov/ij/, 1997–2009). The ImageJ output data were further refined by inspection using a customized Matlab™ image analysis script.

2.5.4. Electron microscopy

Mice were euthanized by cardiac perfusion following asphyxiation with CO_2. Fixative consisted of 2.5% Glutaraldehyde, 2% paraformaldehyde in 0.1 M Na Cacodylate, pH 7.4. Eyes were enucleated, and a wedge shaped slice centered at the ventral midline (~1/6 of retinal area) was sliced from isolated eyecups and subjected to overnight fixation and further processing. Eye slices were post-fixed in 1% OsO_4, and embedded in epon resin following dehydration in graded ethanol. Ultrathin sections were stained with uranyl acetate (3.5% in 50% methanol) and lead citrate. Ultrathin sections were made with a Leica EM UC6 ultramicrocotome (Leica Microsystems, Bannockburn, IL). Images of the sections were acquired with a transmission electron microscope (CM 120, Phillips Biotwin Lens, F.E.I. Company, Hillsboro, OR, USA) coupled to a digital camera (Gatan MegaScan, model 794/20, digital camera (2 K × 2 K), Pleasanton, CA) at the Diagnostic and Research Electron Microscopy Laboratory at UC Davis. Our investigations with EM revealed that many cones of *Opn1sw*$^{Neo/Neo}$ mice in the more ventral retina, where S-opsin normally predominates, had no outer segments or highly disordered outer segments. To assess the morphological differences in the cone outer segments of *Opn1sw*$^{Neo/Neo}$ and WT mice, images of cones were scored on a five-point scale: (1) nearly perfect, parallel outer segment discs; (2) discs largely aligned perpendicular to the outer segment longitudinal axis, but wavy in appearance; (3) some misaligned or incomplete discs that do not fill the outer segment envelope; (4) many misaligned discs often with membrane "blebs"; (5) very highly disordered outer segment structure with vesicles and blebs present and numerous electron-dense membrane inclusions. The rating scale is ordinal, such that cones whose outer segments have higher scores are more seriously disordered.

2.5.5. Cone derived electroretinography

Full field cone-driven electroretinograms (ERGs) were measured with published methods (Lyubarsky, Falsini, Pennesi, Valentini, & Pugh, 1999).

2.5.6. Cone suction pipette recordings

Light responses of mouse cone photoreceptors were recorded with published methods (Nikonov et al., 2006). In brief, the cell body region of one to several cells in the distalmost portion of the outer nuclear layer of a retinal slice was drawn into a suction pipette, and the membrane current measured with a current-to-voltage converter (a form of loose-patch recording). Rod currents were suppressed with a 500 nm rod-saturating background, and

the responses of cones to brief, calibrated flashes of various wavelengths from 340 nm to 630 nm measured. Tissue dissection was performed under IR-illumination. A cautery (Bovie®, Aaron Medical, St. Petersburg, FL) was used to mark the cornea during dissection so that retina orientation could be maintained. To obtain recordings from ventral cones, wedges of retina (~1/8 area of retina) centered at the ventral midline at least 1.0 mm below the optic nerve to the edge of the retina were cut out of the eye cup and chopped into small pieces (~200 μm on a side) with a fine blade.

3. Results

3.1. S-opsin knock-in targeting strategy created a severely hypomorphic allele (*Opn1sw*^{Neo})

3.1.1. Normal Opn1sw transcript is reduced nearly 1000-fold

The insertion of the *Neo*^{R} gene has been frequently reported to cause disruptions in splicing of targeted genes and has thus been exploited to create hypomorphic alleles of various genes (Carmeliet et al., 1996; Jacks et al., 1994; Meyers, Lewandoski, & Martin, 1998; Sleat et al., 2004). The targeting strategy used to create the *Opn1sw*^{Neo} allele inserted the Neomycin resistance (*Neo*^{R}) cassette between the third and fourth exons of the WT gene (Fig. 1a). Correct targeting of *Opn1sw*^{Neo} in ES cells was confirmed with sequencing, PCR and Southern blotting. To assess the effect of the insertion of the *Neo*^{R} cassette on transcription of the *Opn1sw* gene, quantitative real-time PCR (qRT-PCR) was conducted with primers spanning either exons 1–2 or exons 4–5 (Fig. 1a and b). The message level of *Opn1sw* was compared with that of the other two mouse opsin genes, *Rho* (rhodopsin) and *Opn1mw* (M-opsin), with probe sets spanning exons 1–2, and with a fourth probe set for β-actin, using three dilutions of retinal extract (Fig. 1b). In this double logarithmic ($base_2$) plot, upward displacement of the approximately parallel lines through the threshold cycle (C_T) data signifies reduction in message level, with each unit of upward displacement corresponding to a 2-fold reduction. The C_T data of the

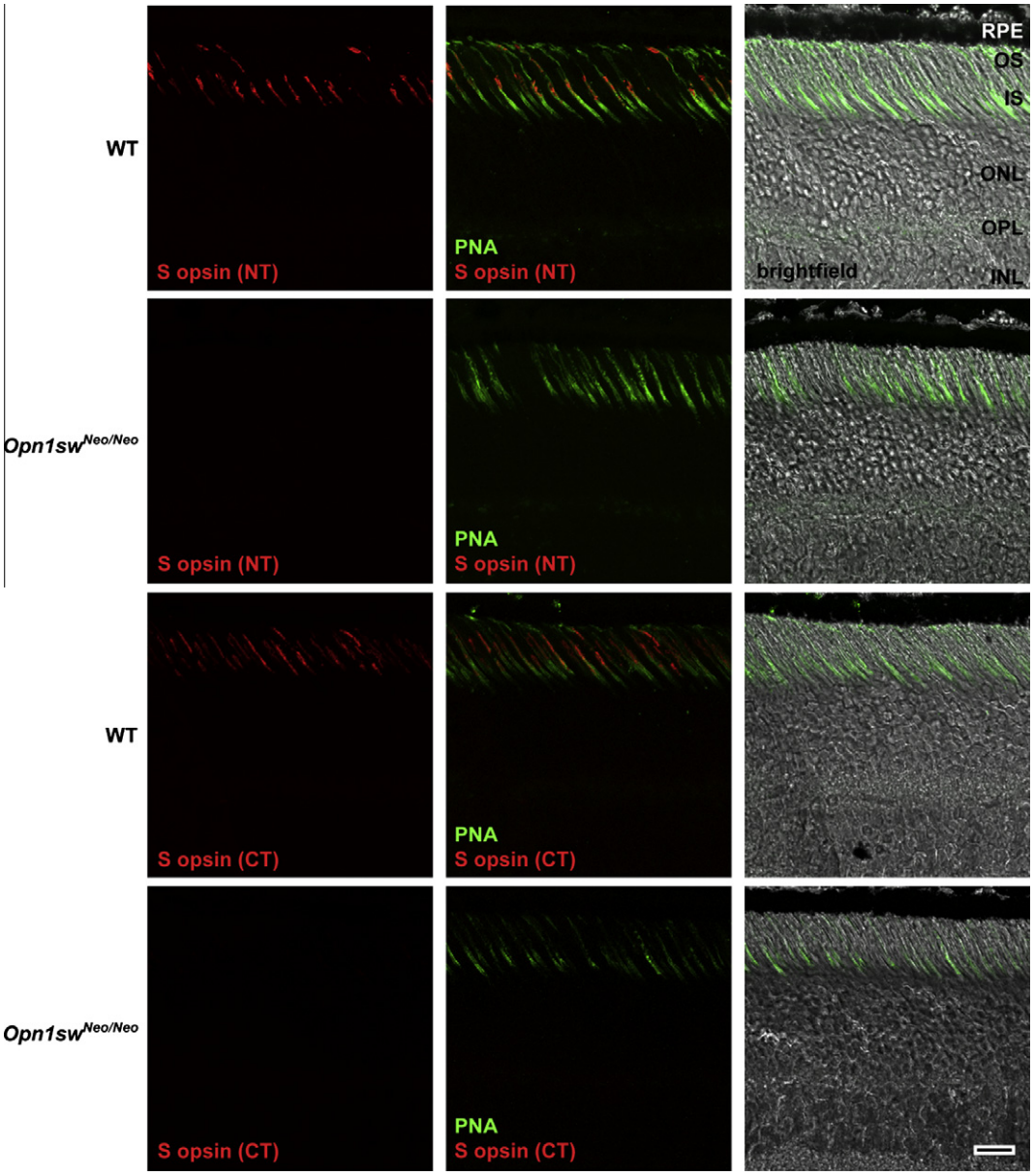

Fig. 2. S-opsin is undetectable histochemically in the *Opn1sw*$^{Neo/Neo}$ retina. Confocal images of cryosections of WT and *Opn1sw*$^{Neo/Neo}$ ventral retina, stained for PNA (green) and S-opsin N-terminal (NT) or C-terminal (CT) antibody (red). The third image in each row superimposes the PNA image on a corresponding brightfield image. Immunoreactivity of S-opsin polypeptides was undetectable in the *Opn1sw*$^{Neo/Neo}$ retina with either N- or C-terminal antibodies. The scale bar, which applies to all panels, represents 20μm.

Opn1sw primer set spanning exons 1–2 showed an ≈4 $\log_2$ step upward displacement, corresponding to a 2^4 = 16-fold reduction relative to WT, indicating that transcription of the S-opsin gene upstream of the *Neo*^{R} cassette is reduced to ~7% of WT. For the *Opn1sw* primer set spanning exons 4–5, however, C_T was increased almost 10 $\log_2$ steps between *Opn1sw*$^{Neo/Neo}$ and WT (Fig. 1b, arrow). No reliable differences between genotypes were observed for the *Opn1mw* and β-actin messages. Taken together, these observations reveal that mRNA for the complete *Opn1sw* gene is reduced $\sim 2^{10} \approx 1000$-fold in the retina of *Opn1sw*$^{Neo/Neo}$ mice.

3.1.2. Several other features of the qRT-PCR data bear emphasis

First, assuming similar efficiencies of the primers, rhodopsin message (average C_T = 16.6 ± 0.6, mean ± sd of all undiluted reactions) exceeds that of β-actin (20.4 ± 0.5) 14-fold, providing a strong rationale for using rhodopsin message to anchor retinal mRNA analysis. Second, the ratio of *Opn1sw* message to *Opn1mw* in the WT retina for both exon 1–2 and exon 3–4 spanning primers is 4–5-fold. This corresponds well with the ratio of sensitivity of the full-field cone-driven electroretinogram b-wave at 360 nm relative to 510 nm, which is interpretable as the relative expression of S-opsin to M-opsin (Lyubarsky et al., 1999). (Because RT-PCR primers can vary in efficiency, comparisons of data obtained with different primers will require further validation to be deemed rigorous.) Third, in WT retina S-opsin mRNA appears present at ~25-fold lower level than that of rhodopsin; this is about 4-fold higher ratio than expected from the overall ratio of total S-opsin to total rhodopsin mass, ~100:1 (Supplement).

A possible concern about the qRT-PCR results arises from evidence that transcription of opsins undergoes circadian oscillations: in mouse retina, S-opsin transcripts are about 3-fold higher at the beginning of the dark phase of a 12:12 LD cycle than at all other times in the cycle (von Schantz, Lucas, & Foster, 1999). The animals used for our qRT-PCR experiments were sacrificed during the late morning, and thus opsin transcripts would be expected to be near the lower level of expression. Circadian variation in the level of opsin transcripts is unlikely to have affected the conclusion, because all opsins appear to have the same circadian cycle in mice, and mRNA from all opsins and animals were collected at the same time of day: thus, transcript ratios, as presented in Fig. 1 should remain valid. Our ultimate concern, however, is with protein products of the *Opn1sw* gene.

3.1.3. S-opsin protein is undetectable in Opn1sw$^{Neo/Neo}$ mice with immunochemical methods

We used two immunochemical approaches to look for protein products of the *Opn1sw*^{Neo} gene: Western blotting and histochemical labeling of cones. Western blotting of *Opn1sw*$^{Neo/Neo}$ retina showed no detectable S-opsin band with a load (60 pmol rhodopsin) that gave a very robust signal from WT retina (Fig. 1c). Calculations indicate that the WT mouse retina has ≈10 pmol total cone opsin in a 1:70 ratio with rhodopsin, with 80% of the cone opsin being S-opsin (Supplement). We estimate that we can detect as little as 30 fmol S-opsin on blots loaded with lysate corresponding to ~1/11th of the whole retina (Supplement, Fig. 1S). This excludes the possibility that the *Opn1sw*$^{Neo/Neo}$ retina has more than 0.33 pmol of the 8 pmol S-opsin present in WT retina, i.e., 4% of the WT level. Likewise, oriented retinal cryosections of *Opn1sw*$^{Neo/Neo}$ mice failed to be labeled by two distinct polyclonal antibodies raised against an N-terminal (Zhu et al., 2003) or C-terminal peptide of mouse S-opsin, while robustly labeling ventral cone outer segments in WT littermate controls (Fig. 2).

In summary, quantitative RT-PCR, Western blot analysis, and immunohistochemical labeling show that the retina of the *Opn1sw*$^{Neo/Neo}$ mouse has no detectable S-opsin, and can thus be classified as an S-opsin knockout.

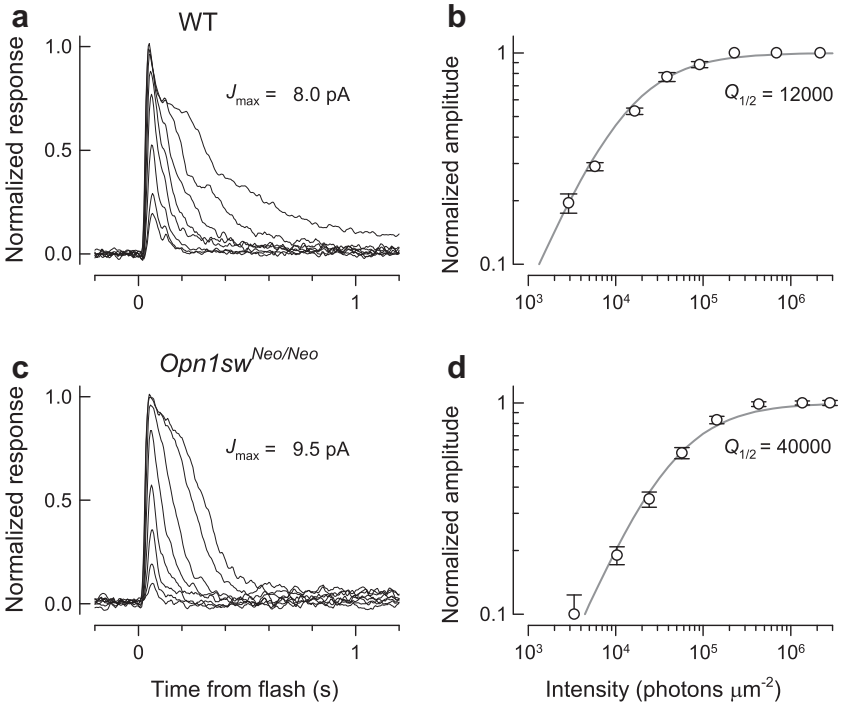

Fig. 3. Response families of WT and *Opn1sw*$^{Neo/Neo}$ Cones: (a and c) *Normalized photocurrents* recorded in response to 10 ms flashes of 500 nm light of graded intensity from an M-opsin dominant cone of the dorsal retina of a WT mouse (a), and an *Opn1sw*$^{Neo/Neo}$ ventral cone (c). (b and d) *Response vs. intensity functions* derived from the corresponding data of panels a, c and plotted and fitted with hyperbolic saturation functions. The quantal energy density ($Q_{1/2}$) of 500 nm light that produces a half-maximal response is indicated on each plot. Flash sensitivity ($1/Q_{1/2}$) extracted from such analyses has units of fraction maximal current per (photon μm^{-2}).

3.2. Cones of the ventral retina of *Opn1sw*$^{Neo/Neo}$ mice respond to light with normal kinetics

Cones of the ventral retina of WT mice primarily express S-opsin, with a small (<10%) fraction of M-opsin co-expression (Applebury et al., 2000; Nikonov et al., 2006; Williams & Jacobs, 2007). Given that retinas of the *Opn1sw*$^{Neo/Neo}$ mouse have no S-opsin, do any or all its ventral cones survive, and if so, do they elaborate functional outer segments? To answer these questions, we used suction electrodes to record light-evoked changes in membrane current of cones of *Opn1sw*$^{Neo/Neo}$ and WT mice. Surprisingly, some ventral cones of the *Opn1sw*$^{Neo/Neo}$ retina gave robust flash responses with normal kinetics (Fig. 3). The maximal sensitivity of *Opn1sw*$^{Neo/Neo}$ ventral cones was invariably at ~510 nm, the λ_{max} of mouse M-opsin (Fig. 4a), whereas in the WT retina the maximum sensitivity of ventral cones was invariably at 360 nm, the λ_{max} of mouse S-opsin, as shown previously (Fig. 4b; see also Nikonov et al., 2006, Fig. 3B). These data confirm the lack of functional expression of S-opsin in the *Opn1sw*$^{Neo/Neo}$ and, more importantly, demonstrate that the absence of this normally dominant cone pigment in the ventral retina is not required to maintain viable cones with functioning outer segments.

3.3. M-opsin expression is elevated in *Opn1sw*$^{Neo/Neo}$ cones of the ventral retina

Another surprising feature of the *Opn1sw*$^{Neo/Neo}$ ventral cones was that they were actually *more* sensitive than WT ventral cones to mid-wavelength light, as revealed by both single cell data (Fig. 4b), and full-field cone-driven ERG recordings (Supplement, Fig. 2S). Comparison of populations of cones revealed that the average sensitivity of *Opn1sw*$^{Neo/Neo}$ ventral cones for 500 nm light was increased 3-fold over that of WT ventral cones ($p < 10^{-4}$; Fig. 4c). These results suggest that M-opsin is expressed at a higher level in *Opn1sw*$^{Neo/Neo}$ ventral cones than in WT ventral cones.

To determine whether M-opsin expression is indeed elevated in the *Opn1sw*$^{Neo/Neo}$ retina, we measured M-opsin expression in whole retina lysates of *Opn1sw*$^{Neo/Neo}$ and WT littermate controls by Western blot (Fig. 5). On average, M-opsin levels were increased 1.6-fold ± 0.25 (mean ± sem; $n = 4$; $p < 0.05$ for test of null hypothesis of no increase, i.e., unit ratio of *Opn1sw*$^{Neo/Neo}$ to WT expression). In these Westerm blot experiments, the quantity of rhodopsin extracted from the *Opn1sw*$^{Neo/Neo}$ eyes did not differ from that of WT littermates (524 ± 44 pmol/eye vs. 516 ± 15 pmol/eye, respectively, mean ± sem), indicating that – exempting cones – the retinas are closely comparable. It seems likely that a substantial fraction of the overall increase occurred in the ventral retina, where M-opsin expression is normally a minor fraction of the opsin in each cone (Fig. 4b; Applebury et al., 2000). Thus, one would expect that the increase in expression in individual *Opn1sw*$^{Neo/Neo}$ ventral cones was considerably higher than the global average increase measured in the whole retinal lysates, since many WT dorsal cones express a full complement of M-opsin. The detailed pattern of increased M-opsin expression across the *Opn1sw*$^{Neo/Neo}$ retina, however, remains an important issue that needs to be addressed experimentally.

3.4. In absence of S-opsin all cones are viable, but outer segments are disordered in a dorso-ventral gradient

3.4.1. Normal cone cell density throughout the retina

To ascertain whether there was any cone cell loss in the *Opn1sw*$^{Neo/Neo}$ retina, we measured cone densities from fluorescence images of peanut agglutinin lectin (PNA)-stained whole mount retinas taken at 0.5 mm intervals along the dorsal–ventral axis (midline) (Fig. 6a); PNA uniquely binds to the extracellular glycoprotein matrix that is secreted by the inner segment of cones (Blanks & Johnson, 1983), and thus indicates cone viability even in the absence of an outer segment. In WT retinas, we counted 12,800 cones per mm^2 along the midline 0.5–2 mm from the optic nerve (Fig. 6c), similar to previous reports (11,000–13,000 mm^{-2}

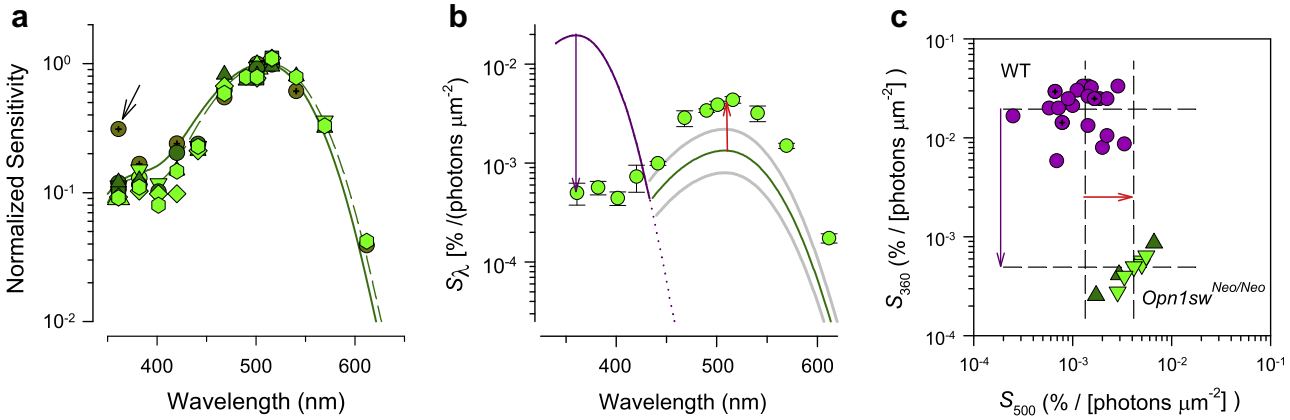

Fig. 4. All cones of *Opn1sw*$^{Neo/Neo}$ mice have the spectral sensitivity of M-opsin: (a) *Normalized spectral sensitivity data.* Different green symbols represent sensitivity of individual single cones from the dorsal (dark green) or ventral retina (light green) of *Opn1sw*$^{Neo/Neo}$ mice; the average data were fitted to normalized templates of 508 nm (solid line) and 510 nm (dashed line) visual pigments (Govardovskii, Fyhrquist, Reuter, Kuzmin, & Donner, 2000; Lamb, 1995). Also shown are data of a single WT M-dominant cone recorded from the dorsal WT retina (dotted olive symbols) that has a similar spectral sensitivity with the exception of 3-fold higher sensitivity at 360 nm (arrow), likely indicating co-expression of S-opsin. (b) *Absolute spectral sensitivity data.* Symbols plot the average absolute spectral sensitivity of *Opn1sw*$^{Neo/Neo}$ cones, expressed as [%/(photons μm^{-2})]. The smooth purple (360 nm pigment template) and green curves (510 nm template) plot the average *absolute* sensitivity of 24 WT ventral cones, mostly from previous studies (Ng et al., 2010; Nikonov et al., 2006), along with 95% confidence bounds (gray curves) for the mid-wave sensitivity derived from this population. The data for the *Opn1sw*$^{Neo/Neo}$ Cones lie outside the confidence bounds, i.e., these ventral cones are more sensitive to mid-wave light than their WT counterparts. The magenta arrow indicates the decrease of sensitivity at 360 nm of *Opn1sw*$^{Neo/Neo}$ ventral cones relative to WT controls, while the red arrow indicates the increase in sensitivity at 510 nm observed in the same experiments. (c) *Scatterplot population statistical analysis.* Sensitivity for 360 nm flashes (S_{360}) is plotted as a function of sensitivity for 500 nm flashes (S_{500}) for populations of WT ventral cones (purple, $n = 24$) including three littermate controls (symbols with cross-hairs), *Opn1sw*$^{Neo/Neo}$ ventral (green, $n = 6$), and *Opn1sw*$^{Neo/Neo}$ dorsal cones (darker green, $n = 3$). The WT population data shows no correlation, as expected if the quantity of M-opsin co-expressed in these cones varied randomly in the sample; in contrast the scatterplot data for the *Opn1sw*$^{Neo/Neo}$ cones is strongly correlated, as expected if a single pigment governs sensitivity. The four dashed lines are drawn through the mean values of the two populations: the magenta and red arrows identify the shifts in sensitivity to 360 nm and 510 nm light for the two populations seen in the spectral sensitivity data of panel b, and correspond exactly in magnitude to the arrows of panel b. Presenting the data in this format enables inspection of the variation in the two populations.

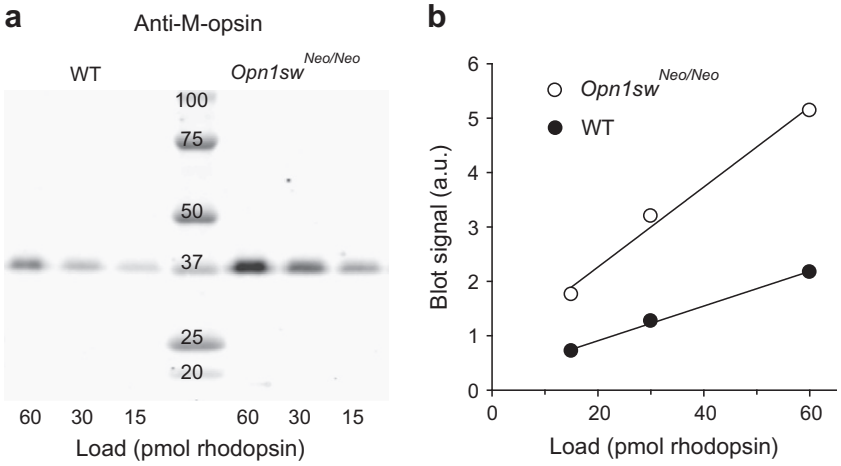

Fig. 5. Immunoblot confirmation of increased M-opsin expression in the *Opn1sw*$^{Neo/Neo}$ retina: (a) *Immunoblots of the M-opsin content of retinas of Opn1sw*$^{Neo/Neo}$ *and WT littermates*. Retinal lysates calibrated in terms of their rhodopsin content were loaded at constant volume into the identified lanes of SDS–PAGE gels and electrophoresed; the PVDF transfer membranes were reacted with a purified, polyclonal M-opsin antibody (Zhu et al., 2003). (A lysate containing 1 pmol rhodopsin corresponds to a total retinal protein mass of 0.24 μg – Section 2.) (b) *Immunoblot intensities* from panel a are plotted as a function of the retinal lysate quantity expressed in rhodopsin mass and fitted with linear regression. The slope of the plot of the *Opn1sw*$^{Neo/Neo}$ data is 2.3-fold steeper than that for the WT littermate's data, indicating an overall 2.3-fold higher level of M-opsin expression in the *Opn1sw*$^{Neo/Neo}$ retina.

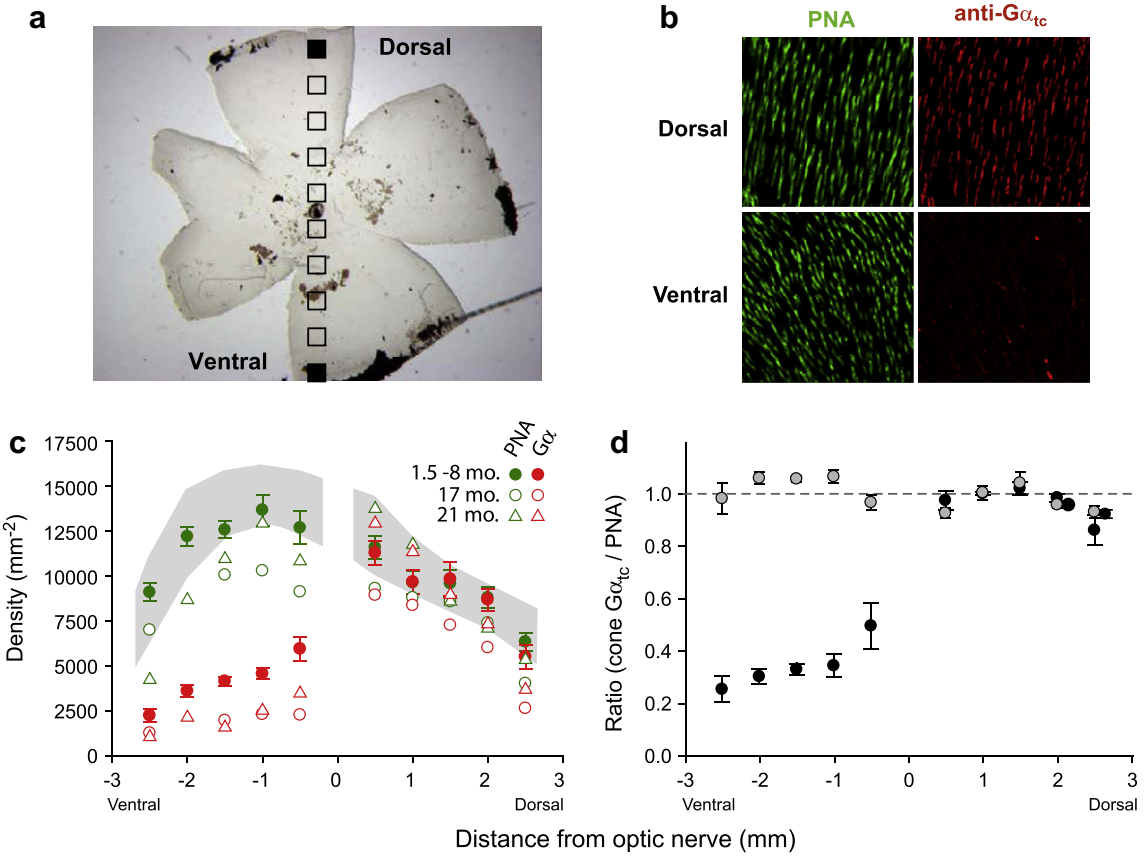

Fig. 6. Immunohistochemistry of *Opn1sw*$^{Neo/Neo}$ retinas reveals all cones to be viable but ventral cones to have reduced cone transducin: (a) *Image of flatmounted Opn1sw*$^{Neo/Neo}$ *retina*, overlaid squares indicating regions (spaced at 0.5 mm intervals) along the dorso-ventral midline axis analyzed for cone densities. (b) *Images of sampled regions at the dorsal and ventral extremes* (filled squares in a) reacted with the lectin peanut agglutinin (PNA, green label) and anti-cone transducin antibody (Gα_{tc}, red label). (c) *Densities* of cones detected with PNA (green symbols) and Gα_{tc} antibody (red symbols) labeling are plotted for five mice of ages 1–8 months as a function of the dorsal (+) or ventral (−) distance from the optic nerve head. Open symbols represent density for two *Opn1sw*$^{Neo/Neo}$ mice of 17 and 21 months respectively. Gray region indicates confidence interval for young WT littermate controls determined from PNA counts. (d) Average ratio of Gα_{tc} to PNA labels along dorso-ventral midline axis of the retina for *Opn1sw*$^{Neo/Neo}$ (black filled circles) and WT littermate controls (gray filled circles). All results reported here were obtained from fully dark adapted mice whose retinas were dissected under infrared illumination to avoid any potential artifact from Gα_{tc} translocation.

(Applebury et al., 2000; Jeon, Strettoi, & Masland, 1998; Williams & Jacobs, 2007). To assess the presence of outer segments in these cones, we compared cells identified by PNA stain with those labeled by an antibody against cone transducin (Gα_{tc}), normally

anchored to the outer segment disc membranes. $G\alpha_{tc}$ label was severely reduced in the ventral half of the retina, with densities falling off steeply within the first mm from the optic nerve and decreasing more gradually as a function of distance thereafter (Fig. 6c and d). The ratio of the densities of the two histochemical labels was close to unity in the dorsal retina, indicating that every PNA-labeled cone had an easily recognized outer segment that was immune-positive for $G\alpha_{tc}$. In the ventral retina, the ratio was strikingly lower, indicating that $G\alpha_{tc}$ staining could not be detected in PNA-labeled cones at this magnification. These results suggest that many of the more ventral cones of the *Opn1sw*$^{Neo/Neo}$ mouse do not elaborate normal outer segments.

3.4.2. A dorso-ventral gradient of rudimentary and disordered outer segments

To characterize the consequences of S-opsin loss at higher resolution, we examined radial sections of the retina with confocal and electron microscopy. Oriented cryosections were examined to investigate whether the loss in $G\alpha_{tc}$ immunoreactivity was due to lower expression of outer segment proteins or total loss of the cone outer segment. Cones were identified on the basis of labeling with PNA and with a polyclonal antibody against the cone-specific arrestin, Arr4, which labels the entire cone (Nikonov et al., 2008; Zhu et al., 2002). Cones of the dorsal retina of *Opn1sw*$^{Neo/Neo}$ mice had completely normal morphology (Fig. 7a), as expected since they are M-opsin dominant in the WT mouse; in contrast, in the ventral retina of *Opn1sw*$^{Neo/Neo}$ mice outer segments were thin, wispy or undetectable with histochemistry (Fig. 7b). Nonetheless, the total number of cones, and the morphology of their cellular compartments other than the outer segment (i.e., the inner segment, cell body, axon and synaptic pedicle) in *Opn1sw*$^{Neo/Neo}$ retinas were indistinguishable from those of WT mice in both dorsal and ventral retina.

Electron microscopy was employed to gain further insight into the nature of the disorder of the outer segments of ventral cones of *Opn1sw*$^{Neo/Neo}$ mice (Fig. 7c–f). Cones in ultrathin sections of mid-ventral retina were distinguished from rods on the basis of previously described structural criteria, namely, the squatter, more rounded profiles of their mitochondria, their wider inner segments and distinct pattern of chromatin condensation (Carter-Dawson & LaVail, 1979; Daniele et al., 2005). To assess the morphological differences in the cone outer segments of *Opn1sw*$^{Neo/Neo}$ and WT mice, images of 16 WT and 9 *Opn1sw*$^{Neo/Neo}$ ventral cones were scored on a five-point scale of disorder, such that the higher the score the more serious the degree of disorder (Section 2) (Fig. 7c–f). WT cones (Supplement, Fig. 3S) scored 1.6 ± 0.23 on average, defining normal overall outer segment morphology. In contrast, *Opn1sw*$^{Neo/Neo}$ ventral cones scored 3.8 ± 0.34: while a few cones were found with nearly normal outer segment morphology (Fig. 7c), many had only rudimentary outer segments whose disorder ranged from mild with narrow, somewhat aligned discs (Fig. 7d and e) to severe, with grossly misaligned discs interrupted by vesicular membrane profiles and occasional large membrane blebs (Fig. 7f). It bears mention in this context that efforts to record light responses from cones in the more ventral *Opn1sw*$^{Neo/Neo}$ retina (much further than 1.5 mm below the optic nerve) were unsuccessful.

4. Discussion

4.1. Creation of a mouse M-opsin cone monochromat

In developing a gene targeting strategy suitable for generating point mutations in the mouse S-opsin gene we created a severely hypomorphic S-opsin allele (*Opn1sw*^{Neo}) whose message is reduced 1000-fold and whose protein expression is undetectable by Western blotting (Fig. 1), histochemistry (Fig. 2), and single-cell recordings (Fig. 3). Given the absence of any detectable S-opsin, the *Opn1sw*$^{Neo/Neo}$ mouse can be classified as an M-opsin cone monochromat.

Two distinctive features of the cone photoreceptors of most rodent retinas including mouse are dorso-ventral counter-gradients of expression of their S- and M-opsins (Szel et al., 2000), and co-expression of the two cone opsins that follow the gradients (Applebury et al., 2000; Nikonov et al., 2006; Szel et al., 2000). These dorso-ventral gradients have been shown to be governed by several hormonal regulatory enzymes, and transcription factors (Ng et al., 2001, 2010; Roberts, Hendrickson, McGuire, & Reh, 2005; Roberts, Srinivas, Forrest, Morreale de Escobar, & Reh, 2006). The dorso-ventral positional dependence of cone opsin co-expression complicates the analysis of cone phototransduction (Nikonov et al., 2005, 2006, 2008) and analysis of other aspects of cone vision in mice (Naarendorp et al., 2010), but also provides a useful preparation for investigating the machinery regulating cone opsin translation, and trafficking (Avasthi et al., 2009), and outer segment formation, as we now discuss.

4.2. Why do cones survive despite the loss of S-opsin when rods die in the absence of rhodopsin?

Our results show that all mouse cones survive in the absence of S-opsin, even in the ventral retina (Fig. 6) where S-opsin normally predominates. In contrast, when rhodopsin expression is genetically eliminated (*Rho*$^{-/-}$ mice), rods do not form outer segments, and undergo apoptosis by 2.5 months (Humphries et al., 1997; Lee et al., 2006). A partial explanation of this striking difference between the fate of rods in *Rho*$^{-/-}$ retinas and ventral cones in *Opn1sw*$^{Neo/Neo}$ mice is that M-opsin expression may enable sufficient membrane trafficking to support formation of cone outer segments (Fig. 7). While M-opsin expression no doubt does support the formation of functional outer segments in many ventral cones, the fact remains that a substantial fraction of ventral cones in *Opn1sw*$^{Neo/Neo}$ mice survive without an outer segment: at the EM level such cones have severely disordered rudimentary outer segments (Fig. 7), which resemble the outer segments of rods of *Rho*$^{-/-}$ mice at P30 just prior to the onset of rod degeneration (Lee et al., 2006).

Why then do cones with no detectable outer segments in *Opn1sw*$^{Neo/Neo}$ mice survive into adulthood when rods of *Rho*$^{-/-}$ mice have largely died by P90? Perhaps the absence of an outer segment *per se* is not deleterious, and cell death in rods is caused by an indirect effect. Cone cells survive in the absence of outer segments at least a month after experimental retinal detachment; initially after detachment, cones rapidly lose their outer segments and stop synthesizing most proteins that are targeted there (Linberg, Lewis, Shaaw, Rex, & Fisher, 2001; Rex et al., 2002). Because rods are the predominant cell type of the outer retina, the loss of their outer segments will indirectly produce structural and functional (e.g., Yu et al., 2004) changes in the subretinal space which lies between the retinal pigment epithelium and the outer limiting membrane. Since mouse cones comprise only 3% of retinal photoreceptors, loss of even a large portion of their outer segments should minimally affect the structure and physiological properties of the outer retina.

The relative hardiness of cones is highlighted by an important recent investigation in which AAV-mediated transfer of a light-sensitive photoactivatable chloride pump restored cone light responsivity in retinas with rod-based retinal degeneration: though the cone outer segments were negligible, the transfected cones generated light-sensitive hyperpolarizing currents that could drive responses in inner retinal neurons (Busskamp et al., 2010).

4.3. The increased M-opsin expression in the Opn1sw$^{Neo/Neo}$ retina can be explained from removal of competition from S-opsin transcripts

The loss of S-opsin expression in the *Opn1sw*$^{Neo/Neo}$ retina produced several unanticipated physiological effects, including some ventral cones expressing only M-opsin with normal response kinetics (Fig. 3) and increased sensitivity to mid-wave light (Fig. 4b and c). The driving force behind these changes appears to be an increased expression of M-opsin protein without a significant change in its rate of transcription (Figs. 1 and 5). The increase in M-opsin expression may arise because S- and M-opsin mRNA must compete for the same ribosomal translational machinery in cones where they are both expressed. Thus, the effective absence of S-opsin transcripts in *Opn1sw*$^{Neo/Neo}$ cones could result in higher M-opsin expression without any change in the transcription of the gene.

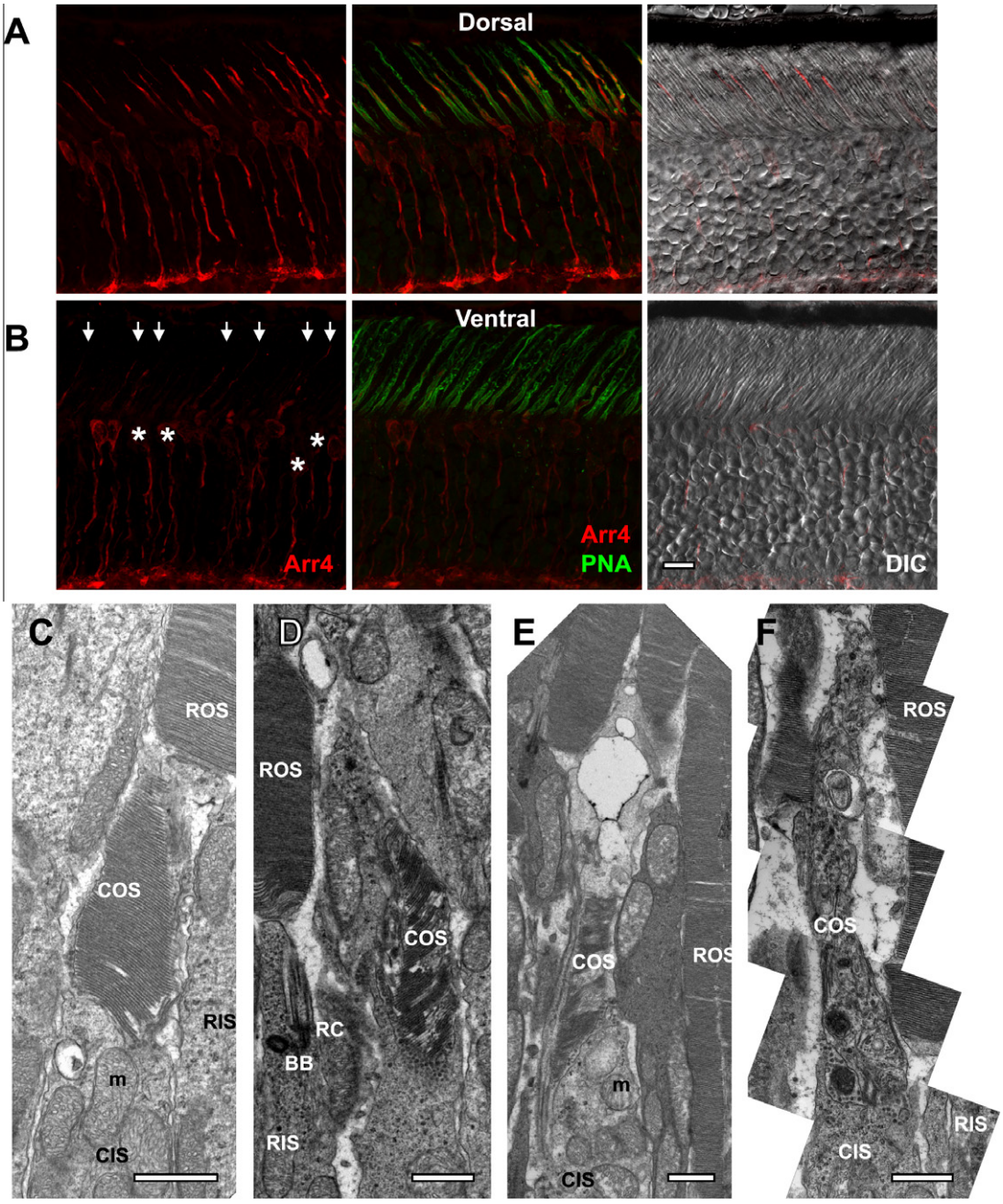

Fig. 7. High resolution histology of *Opn1sw*$^{Neo/Neo}$ mouse retina reveals a dorso-ventral gradient of outer segment disorder: (a and b) *Confocal images of cryosections of an Opn1sw*$^{Neo/Neo}$ *mouse eye (age 1 month) taken along the dorso-ventral midline axis.* Left panels show labeling for antibody raised against mouse cone arrestin (Arr4, red); middle panels show PNA labeling (green) with Arr4 overlay (red); right panels show DIC images of same fields with Arr4 immunofluorescence overlay (red). White arrows in the bottom left panel point to outer segments that appear "wispy" (unusually thin) at this level of resolution, while asterisks indicate cones with no detectable outer segments. [Abbreviations: RPE, retinal pigment epithelial layer; OS, outer segment; IS, inner segment; ONL, outer nuclear layer; OPL; outer plexiform layer. Scale bar, 10 μm.] (c–f) *EM images of representative ventral cone profiles from two Opn1sw*$^{Neo/Neo}$ *mice, aged 6 months.* Cone images were scored on a scale of least (1) to greatest (5) outer segment disorder (Section 2), and arranged accordingly (c, score = 2; d, score = 3; e, score = 4; f, score = 5). *Opn1sw*$^{Neo/Neo}$ ventral cones scored 3.8 on average (±0.34, $n = 9$) while WT cones scored 1.6 (±0.23, $n = 16$). [Abbreviations: BB, basal body; CIS, cone inner segment; COS, cone outer segment; m, mitochondria; RC, rod cilium; RIS, rod inner segment; ROS, rod outer segment. Scale bar, 1 μm.] Images of WT littermate control cones are illustrated in Fig. 3S of the Supplement.

To examine these ideas, we developed a model of the dual dorso-ventral gradients of S- and M-opsin expression in WT retina described by Applebury et al. (2000) (Fig. 8; Supplement). This analysis was inspired by recent investigations showing that translation of most transcripts in cells obeys rate-limited (Michaelis) kinetics (Brockmann, Beyer, Heinisch, & Wilhelm, 2007). As a consequence, it can be expected that highly abundant transcripts such as that of rhodopsin in rods or of S-opsin in cones (Fig. 1b) would act as inhibitors of the translation of other less abundant transcripts, reducing their access to the ribosomal translation machinery. Assuming that the transcripts of the two cone opsins have equal affinity for the ribosomes and that the summed concentration of the two transcripts exceeds the K_m for translation by ~2-fold, the model predicts a 1.8-fold global increase in M-opsin expression, which is very similar to the 1.6-fold increase observed (Fig. 5). Furthermore, the model predicts that this increase in expression should result in an almost 3-fold maximal increase in mid-wave light sensitivity in *Opn1sw*$^{Neo/Neo}$ as compared to WT ventral cones (Fig. 8c), close to the observed experimental average (Fig. 4b and c). However, we also observed that the ventral-most *Opn1sw*$^{Neo/Neo}$ cones did not make outer segments at all, presumably because of inadequate total opsin expression and membrane trafficking. Can we deduce from our observations a minimum opsin expression level necessary for cone outer segment formation?

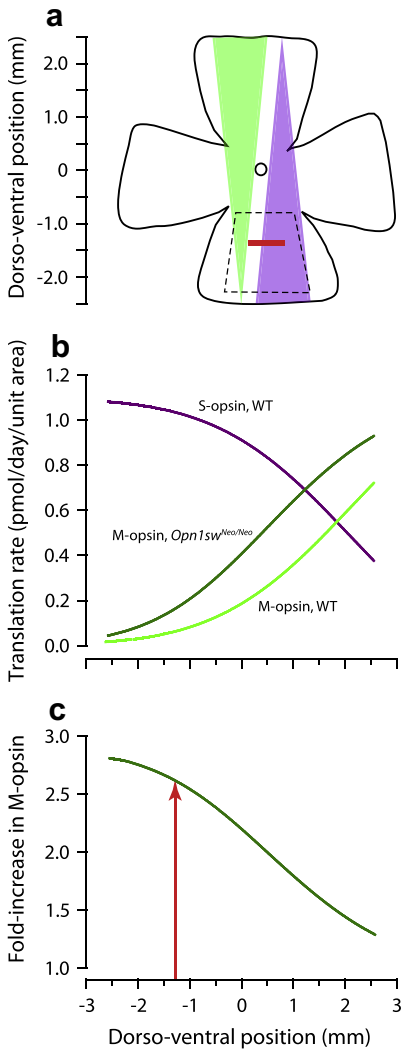

Fig. 8. Increased M-opsin expression in *Opn1sw*$^{Neo/Neo}$ is predicted as a relief of competition by S-opsin transcripts of M-opsin translation. (a) Schematic of a flat-mounted mouse retina giving proper scale (~5 mm from dorsal to ventral edges). The colored wedges schematize the dorso-ventral gradients of M-opsin and S-opsin co-expression in the WT mouse cones, with M-opsin declining dorsal to ventral, and S-opsin following a countergradient pattern. As cone outer segments are uniform in size throughout the retina, all cones likely express the same total quantity of opsin. The dashed region in the ventral retina outlines the portion of the retina from which slices are taken in experiments involving ventral retina; the red bar represents the mid-ventral locus on the dorso-ventral axis. For interpretation of panels b, c, note that ventral positions are negative and dorsal positive. (b) Rates of translation of S-opsin (magenta lines) and M-opsin (light-green lines) in WT and of M-opsin (dark green lines) in *Opn1sw*$^{Neo/Neo}$ retinas, as a function of the dorso-ventral position. Rates are calculated with the model described in Supplement; the spatially integrated (over the whole retina) rate corresponds to 1.1 pmol/day of cone opsin. The increased rate of translation of M-opsin in the *Opn1sw*$^{Neo/Neo}$ is an exclusive consequence of the elimination of S-opsin transcripts. Integrated over the whole retina, the predicted increase in M-opsin expression is 1.8-fold. Fold-increase in M-opsin expression in the *Opn1sw*$^{Neo/Neo}$ retina relative to WT M-opsin, expression as a function of the dorso-ventral position. The intersection of the red arrow with the curve gives the predicted increase (1.6-fold) in sensitivity of *Opn1sw*$^{Neo/Neo}$ mid-ventral cones over their WT counterparts.

4.4. Minimum opsin expression level for formation of cone outer segments

The minimum opsin expression level for the formation of functional outer segments can be estimated from our results in two ways. First, consider a retina divided into dorsal and ventral sectors with roughly equal numbers of cones, with M-opsin comprising 20% of the total cone opsin. Assuming the measured 60% global increase in M-opsin expression in the *Opn1sw*$^{Neo/Neo}$ retina occurred exclusively in the ventral sector, then ventral cones would have on average $[(0.2 \times 0.6)/0.5] \times 100 = 24\%$ of their normal total complement of opsin. This oversimplified dorso-ventral gradient description reveals the maximum M-opsin that could be expressed in the most ventral *Opn1sw*$^{Neo/Neo}$ cones, and thus is an upper limit for the threshold for outer segment formation. A second estimate can be made from the electrophysiological measures of spectral sensitivity (Fig. 3). The light-responsive cones of *Opn1sw*$^{Neo/Neo}$ ventral retina were 22 ± 11% (mean ± sem) as sensitive to mid-wave light as WT ventral cones were to short-wave light (Fig. 4b and c), suggesting that these *Opn1sw*$^{Neo/Neo}$ ventral cones express on average about 20% of WT levels of total cone opsin. In addition, given that the average sensitivity of ventral WT cones for 510 nm light is 6.5% that of their sensitivity for 360 nm light (Fig. 4b), a 2.6-fold increase in M-opsin expression in the mid-ventral retina (Fig. 8c) would cause the sensitivity of the electrically responsive *Opn1sw*$^{Neo/Neo}$ ventral cones to increase to $2.6 \times 6.5\% = 17\%$ of the WT sensitivity at 360 nm, close to the observed value of 20%. The calculations based on the electrophysiological data assume that the measured sensitivity at a specific wavelength is proportional to the total quantity of opsin in the outer segment, multiplied by the specific spectral sensitivity of the pigment at that wavelength, and that S- and M-opsins activate phototransduction equally. Our observations thus lead to the conclusion that stably functional cone outer segments can be generated with 20% or lower opsin levels relative to normal. A similar rule likewise appears to hold for the formation of rod outer segments: in one study rods of rhodopsin-null (*Rho*$^{-/-}$) mice expression of M-opsin at a level of 11% that of rhodopsin supported formation of outer segments that were electrically light-responsive (Sakurai et al., 2007); in another study, expression of S-opsin in *Rho*$^{-/-}$ rods at a level of ~13% that of rhodopsin produced healthy cells with robust responses (Shi, Yau, Chen, & Kefalov, 2007).

Acknowledgments

We are grateful to Marie Burns and Barry Knox for helpful comments, to Cheryl Craft for providing antibodies and to Paul Fitzgerald and Brad Shibata for assistance with electron microscopy.

Supported by NIH EY02660, NIH EY012576 (core grant) and T32 NIH EY15387 (training grant).

Appendix A. Supplementary material

Supplementary data associated with this article can be found, in the online version, at doi:10.1016/j.visres.2010.12.017.

References

Applebury, M. L., Antoch, M. P., Baxter, L. C., Chun, L. L., Falk, J. D., Farhangfar, F., et al. (2000). The murine cone photoreceptor: A single cone type expresses both S and M opsins with retinal spatial patterning. *Neuron, 27*(3), 513–523.

Avasthi, P., Watt, C. B., Williams, D. S., Le, Y. Z., Li, S., Chen, C. K., et al. (2009). Trafficking of membrane proteins to cone but not rod outer segments is dependent on heterotrimeric kinesin-II. *Journal of Neuroscience, 29*(45), 14287–14298.

Blanks, J. C., & Johnson, L. V. (1983). Selective lectin binding of the developing mouse retina. *Journal of Comparative Neurology, 221*(1), 31–41.

Bradford, M. M. (1976). A rapid and sensitive method for the quantitation of microgram quantities of protein utilizing the principle of protein-dye binding. *Analytical Biochemistry, 72*, 248–254.

Brockmann, R., Beyer, A., Heinisch, J. J., & Wilhelm, T. (2007). Posttranscriptional expression regulation: What determines translation rates? *PLoS Computational Biology, 3*(3), e57.

Busskamp, V., Duebel, J., Balya, D., Fradot, M., Viney, T. J., Siegert, S., et al. (2010). Genetic reactivation of cone photoreceptors restores visual responses in retinitis pigmentosa. *Science, 329*(5990), 413–417.

Carmeliet, P., Ferreira, V., Breier, G., Pollefeyt, S., Kieckens, L., Gertsenstein, M., et al. (1996). Abnormal blood vessel development and lethality in embryos lacking a single VEGF allele. *Nature, 380*(6573), 435–439.

Carter-Dawson, L. D., & LaVail, M. M. (1979). Rods and cones in the mouse retina. I. Structural analysis using light and electron microscopy. *Journal of Comparative Neurology, 188*(2), 245–262.

Daniele, L. L., Lillo, C., Lyubarsky, A. L., Nikonov, S. S., Philp, N., Mears, A. J., et al. (2005). Cone-like morphological, molecular, and electrophysiological features of the photoreceptors of the Nrl knockout mouse. *Investigative Ophthalmology and Visual Science, 46*(6), 2156–2167.

Govardovskii, V. I., Fyhrquist, N., Reuter, T., Kuzmin, D. G., & Donner, K. (2000). In search of the visual pigment template. *Visual Neuroscience, 17*(4), 509–528.

Hollyfield, J. G. (1979). Membrane addition to photoreceptor outer segments: Progressive reduction in the stimulatory effect of light with increased temperature. *Investigative Ophthalmology and Visual Science, 18*(9), 977–981.

Humphries, M. M., Rancourt, D., Farrar, G. J., Kenna, P., Hazel, M., Bush, R. A., et al. (1997). Retinopathy induced in mice by targeted disruption of the rhodopsin gene. *Nature Genetics, 15*(2), 216–219.

Jacks, T., Shih, T. S., Schmitt, E. M., Bronson, R. T., Bernards, A., & Weinberg, R. A. (1994). Tumour predisposition in mice heterozygous for a targeted mutation in Nf1. *Nature Genetics, 7*(3), 353–361.

Jeon, C. J., Strettoi, E., & Masland, R. H. (1998). The major cell populations of the mouse retina. *Journal of Neuroscience, 18*(21), 8936–8946.

Laird, D. W., & Molday, R. S. (1988). Evidence against the role of rhodopsin in rod outer segment binding to RPE cells. *Investigative Ophthalmology and Visual Science, 29*(3), 419–428.

Lamb, T. D. (1995). Photoreceptor spectral sensitivities: Common shape in the long-wavelength region. *Vision Research, 35*(22), 3083–3091.

Lee, E. S., Burnside, B., & Flannery, J. G. (2006). Characterization of peripherin/rds and rom-1 transport in rod photoreceptors of transgenic and knockout animals. *Investigative Ophthalmology and Visual Science, 47*(5), 2150–2160.

Linberg, K. A., Lewis, G. P., Shaaw, C., Rex, T. S., & Fisher, S. K. (2001). Distribution of S- and M-cones in normal and experimentally detached cat retina. *Journal of Comparative Neurology, 430*(3), 343–356.

Lyubarsky, A. L., Daniele, L. L., & Pugh, E. N. Jr., (2004). From candelas to photoisomerizations in the mouse eye by rhodopsin bleaching in situ and the light-rearing dependence of the major components of the mouse ERG. *Vision Research, 44*(28), 3235–3251.

Lyubarsky, A. L., Falsini, B., Pennesi, M. E., Valentini, P., & Pugh, E. N. Jr., (1999). UV- and midwave-sensitive cone-driven retinal responses of the mouse: A possible phenotype for coexpression of cone photopigments. *Journal of Neuroscience, 19*(1), 442–455.

Meyers, E. N., Lewandoski, M., & Martin, G. R. (1998). An Fgf8 mutant allelic series generated by Cre- and Flp-mediated recombination. *Nature Genetics, 18*(2), 136–141.

Naarendorp, F., Esdaille, T. M., Banden, S. M., Andrews-Labenski, J., Gross, O., & Pugh, E. N. Jr., (2010). Dark light, rod saturation and the absolute and incremental sensitivity of mouse cone vision. *Journal of Neuroscience, 30*(37), 12.

Ng, L., Hurley, J. B., Dierks, B., Srinivas, M., Salto, C., Vennstrom, B., et al. (2001). A thyroid hormone receptor that is required for the development of green cone photoreceptors. *Nature Genetics, 27*(1), 94–98.

Ng, L., Lyubarsky, A., Nikonov, S. S., Ma, M., Srinivas, M., Kefas, B., et al. (2010). Type 3 deiodinase, a thyroid-hormone-inactivating enzyme, controls survival and maturation of cone photoreceptors. *Journal of Neuroscience, 30*(9), 3347–3357.

Nikonov, S. S., Brown, B. M., Davis, J. A., Zuniga, F. I., Bragin, A., Pugh, E. N. Jr.,, et al. (2008). Mouse cones require an arrestin for normal inactivation of phototransduction. *Neuron, 59*(3), 462–474.

Nikonov, S. S., Daniele, L. L., Zhu, X., Craft, C. M., Swaroop, A., & Pugh, E. N. Jr., (2005). Photoreceptors of $Nrl^{-/-}$ mice coexpress functional S- and M-cone opsins having distinct inactivation mechanisms. *Journal of General Physiology, 125*(3), 287–304.

Nikonov, S. S., Kholodenko, R., Lem, J., & Pugh, E. N. Jr., (2006). Physiological features of the S- and M-cone photoreceptors of wild-type mice from single-cell recordings. *Journal of General Physiology, 127*(4), 359–374.

Rex, T. S., Fariss, R. N., Lewis, G. P., Linberg, K. A., Sokal, I., & Fisher, S. K. (2002). A survey of molecular expression by photoreceptors after experimental retinal detachment. *Investigative Ophthalmology and Visual Science, 43*(4), 1234–1247.

Roberts, M. R., Hendrickson, A., McGuire, C. R., & Reh, T. A. (2005). Retinoid X receptor (gamma) is necessary to establish the S-opsin gradient in cone photoreceptors of the developing mouse retina. *Investigative Ophthalmology and Visual Science, 46*(8), 2897–2904.

Roberts, M. R., Srinivas, M., Forrest, D., Morreale de Escobar, G., & Reh, T. A. (2006). Making the gradient: Thyroid hormone regulates cone opsin expression in the developing mouse retina. *Proceedings of the National Academy of Science (USA), 103*(16), 6218–6223.

Sakurai, K., Onishi, A., Imai, H., Chisaka, O., Ueda, Y., Usukura, J., et al. (2007). Physiological properties of rod photoreceptor cells in green-sensitive cone pigment knock-in mice. *Journal of General Physiology, 130*(1), 21–40.

Shi, G., Yau, K. W., Chen, J., & Kefalov, V. J. (2007). Signaling properties of a short-wave cone visual pigment and its role in phototransduction. *Journal of Neuroscience, 27*(38), 10084–10093.

Sleat, D. E., Wiseman, J. A., El-Banna, M., Kim, K. H., Mao, Q., Price, S., et al. (2004). A mouse model of classical late-infantile neuronal ceroid lipofuscinosis based on targeted disruption of the CLN2 gene results in a loss of tripeptidyl-peptidase I activity and progressive neurodegeneration. *Journal of Neuroscience, 24*(41), 9117–9126.

Szel, A., Lukats, A., Fekete, T., Szepessy, Z., & Rohlich, P. (2000). Photoreceptor distribution in the retinas of subprimate mammals. *Journal of the Optical Society of America A – Optics Image Science and Vision, 17*(3), 568–579.

von Schantz, M., Lucas, R. J., & Foster, R. G. (1999). Circadian oscillation of photopigment transcript levels in the mouse retina. *Brain Research. Molecular Brain Research, 72*(1), 108–114.

Wagner, E., McCaffery, P., & Drager, U. C. (2000). Retinoic acid in the formation of the dorsoventral retina and its central projections. *Developmental Biology, 222*(2), 460–470.

Williams, G. A., & Jacobs, G. H. (2007). Cone-based vision in the aging mouse. *Vision Research, 47*(15), 2037–2046.

Young, R. W. (1967). The renewal of photoreceptor cell outer segments. *Journal of Cell Biology, 33*(1), 61–72.

Young, R. W. (1971). The renewal of rod and cone outer segments in the rhesus monkey. *Journal of Cell Biology, 49*(2), 303–318.

Yu, D. Y., Cringle, S., Valter, K., Walsh, N., Lee, D., & Stone, J. (2004). Photoreceptor death, trophic factor expression, retinal oxygen status, and photoreceptor function in the P23H rat. *Investigative Ophthalmology and Visual Science, 45*(6), 2013–2019.

Zhang, H., Fan, J., Li, S., Karan, S., Rohrer, B., Palczewski, K., et al. (2008). Trafficking of membrane-associated proteins to cone photoreceptor outer segments requires the chromophore 11-cis-retinal. *Journal of Neuroscience, 28*(15), 4008–4014.

Zhang, P., Li, M. Z., & Elledge, S. J. (2002). Towards genetic genome projects: Genomic library screening and gene-targeting vector construction in a single step. *Nature Genetics, 30*(1), 31–39.

Zhu, X., Brown, B., Li, A., Mears, A. J., Swaroop, A., & Craft, C. M. (2003). GRK1-dependent phosphorylation of S and M opsins and their binding to cone arrestin during cone phototransduction in the mouse retina. *Journal of Neuroscience, 23*(14), 6152–6160.

Zhu, X., Li, A., Brown, B., Weiss, E. R., Osawa, S., & Craft, C. M. (2002). Mouse cone arrestin expression pattern: Light induced translocation in cone photoreceptors. *Molecular Vision, 8*, 462–471.

Znoiko, S. L., Rohrer, B., Lu, K., Lohr, H. R., Crouch, R. K., & Ma, J. X. (2005). Downregulation of cone-specific gene expression and degeneration of cone photoreceptors in the $Rpe65^{-/-}$ mouse at early ages. *Investigative Ophthalmology and Visual Science, 46*(4), 1473–1479.